JOINT EUROPEAN TORUS

JET–P(90)16

D.P. Schissel, J.C. DeBoo, K.H. Burrell, J.R. Ferron, R.J. Groebner, H. St. John, R.D. Stambaugh, B.J.D. Tubbing, K. Thomsen, J.G. Cordey, M. Keilhacker, D. Stork, P.E. Stott, A. Tanga and JET Team

H-Mode Energy Confinement Scaling from the DIII-D and JET Tokamaks

H-Mode Energy Confinement Scaling from the DIII-D and JET Tokamaks

D.P. Schissel[1], J.C. DeBoo[1], K.H. Burrell[1], J.R. Ferron[1], R.J. Groebner[1], H. St. John[1], R.D. Stambaugh[1], B.J.D. Tubbing[2], K. Thomsen[2], J.G. Cordey[2], M. Keilhacker[2], D. Stork[2], P.E. Stott[2], A. Tanga2 and JET Team*

JET-Joint Undertaking, Culham Science Centre, OX14 3DB, Abingdon, UK

** See Appendix 1*

Preprint of Paper to be submitted for publication in
Nuclear Fusion

ABSTRACT.

Neutral beam heated H-mode DIII-D and JET expanded boundary divertor discharges were examined to study the parametric dependence of the thermal energy confinement on the plasma current, plasma size and neutral beam power. Single-null discharges in both machines were examined during the ELM-free phase (ELM stands for edge localized mode) to extract information about the intrinsic H-mode thermal energy confinement time τ_{th}. A power law dependence of ELM-free thermal energy confinement was assumed, with the result that for $B_T \approx 2.2T$ and $\kappa = 1.8$, $\tau_{th} = C\ I_p^{1.03\pm0.07}\ P_L^{-0.46\pm0.06}\ L^{1.48\pm0.09.}$ The size dependence of τ_{th} is described by the linear dimension L since the determination of the individual α and R dependences on the minor and major radii is precluded by the similar aspect ratio of the two machines. For this representation of τ_{th} (units of MA, MW and m), when L is the plasma major radius, $C = 0.106 \pm 0.011$, and when L is the plasma minor radius, $C = 0.441 \pm 0.044$. A dimensionally correct version of the scaling, consistent with the constraints of a collisional high β beta model, is $\tau_{th} \propto I_p^{1.06}\ P_L^{-0.45}\ L^{1.40}\ n_e^{0.07}\ B_T^{0.06}$. These results indicate that, within the experimental error, the empirical scaling and the dimensionally correct scaling are the same.

1. INTRODUCTION

In the designs of next step tokamak machines that are presently under discussion, energy confinement (τ_E) has been identified as a critical parameter [1]. The indications are that were these machines to operate in the conventional L–mode regime they would either not ignite or have a small ignition margin. These predictions are based on application of various empirical scalings [2–5] that have been created for the L–mode regime. However, with the discovery of the H–mode on ASDEX [6] and the confirmation of this enhanced confinement regime on other tokamaks [7–10], tokamak design studies have assumed the ability to obtain better than L–mode confinement. The predictions for H–mode confinement in next generation devices have been based on the use of numerous L–mode τ_E scaling expressions with an H–mode enhancement factor of order two. There is, however, no reason to assume that the physics underlying the confinement enhancement in the H–mode is the same as the physics underlying the basic L–mode confinement, and therefore no a priori reason why the global confinement scaling should be similar for the two regimes. The H–mode confinement enhancement is believed to be at least partly caused by the formation of a transport barrier at the plasma edge. However, decreases of the transport parameters throughout the bulk of the plasma have also been observed [11,12].

A genuine empirical H–mode scaling for τ_E, based on H–mode data from more than one machine, does not exist. In this paper, we present the results of an initial attempt at creating an H–mode confinement scaling based on H–mode data from the DIII–D and JET tokamaks. Specifically, we investigated how ELM-free H–mode thermal energy confinement (τ_{th}) depends on plasma size, plasma current (I_p) and absorbed neutral beam power (P_b). The dependence of H–mode τ_{th} on plasma current

and neutral beam power is relatively easy to obtain for any given tokamak. However, divertor H–mode size scaling experiments in one tokamak are very difficult to perform due to the difficulties associated with controlling the plasma shape as the plasma size is reduced. In order to overcome this difficulty, JET and DIII–D H–mode discharges of similar shape and with similar dependencies of τ_{th} on P_b and I_p have been combined to obtain the size dependence of τ_{th}. Since the aspect ratio of the two machines is the same it was not possible to establish the individual major (R) and minor radius (a) dependence of τ_{th}. Instead, the effect of plasma size on τ_{th} was represented by a function of a characteristic plasma linear dimension L. Since the plasma magnetic field (B_T), elongation (κ), and aspect ratio (R/a) have been kept constant during this comparison, no information on the dependence of τ_{th} on these parameters was obtained.

H–mode energy confinement can be considered in two different regimes, namely in the presence of edge localized modes (ELMs) or in their absence. One major difference between the H–mode in the two tokamaks was the frequent occurrence of ELMs in DIII–D compared with their relative absence in JET. This difference in H–mode behavior is illustrated by examining the traces of the total stored energy and the D_α emission in Fig. 1. The first graph represents the evolution of a high power DIII–D H–mode that begins to ELM after a short ELM–free phase. The second and third graphs illustrate for both a DIII–D (low power) and JET discharge an H–mode without ELMs. Previous confinement results from DIII–D [13] have been obtained during the ELMing phase of the H–mode which would occur around 2.6 s in the first graph of Fig. 1. These results indicated that deuterium H–mode τ_E with ELMs increased with increasing plasma current for $q_{95} \geq 3$ and decreased with increasing total power (P_T). The total power is defined as the sum of the neutral beam power minus shinethrough plus the ohmic heating power. Recently reported JET results [14] have been obtained by examining ELM–free deuterium H–mode discharges similar in behavior to the plasma presented in the third graph of Fig. 1. These JET results

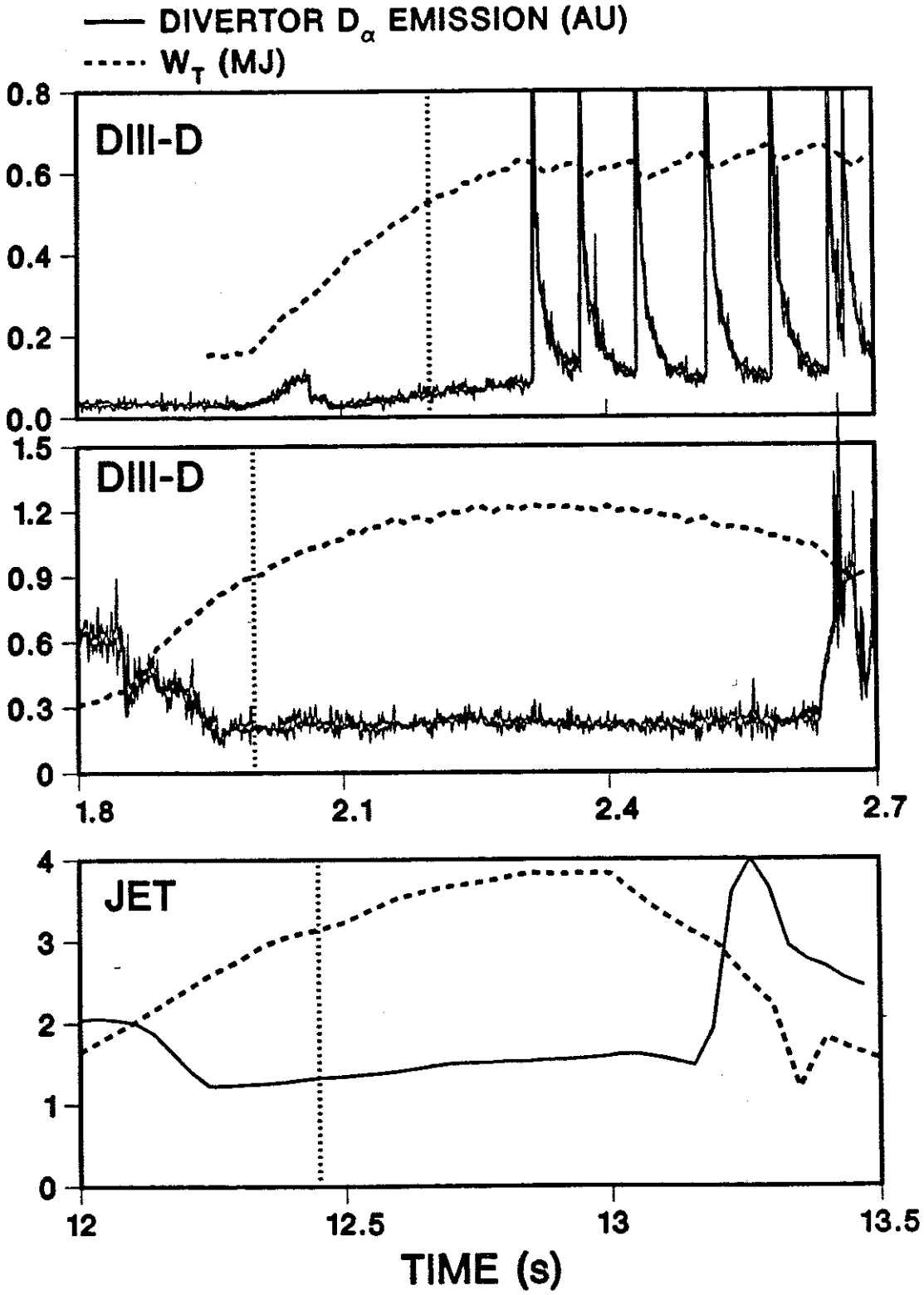

Fig. 1. Stored energy and D_α signals for two DIII–D H–modes and one JET H–mode illustrating different ELM behavior. The dotted vertical line indicates when $\dot{W}_T/P_T \approx 0.3$, and therefore the time when the energy confinement time was calculated.

indicated that $\tau_E \sim I_p^{0.76} n_e^{0.18} P_L^{-0.69} B_T^{0.48}$ where n_e is the electron density and P_L is the loss power defined as the total input power minus the time rate of change of the total plasma stored energy $\dot{W}_T$. The weaker than linear JET current dependence resulted from the inclusion of data with $q_{95} \leq 3.0$ along with the non–optimization of the highest current discharges.

The effect of ELMs on DIII–D [15] has been the reduction in impurity accumulation resulting in quasi–steady state H–mode operation. However ELMs also produce a modest, although difficult to quantify, reduction in the time averaged particle and energy confinement. The confinement analysis for the present study has been limited to the ELM–free periods following the L–H transition. These analysis times are illustrated in Fig. 1 by the dotted vertical lines. This choice of ELM–free data eliminated the ELM related differences between tokamaks, eliminated the need to quantify ELM effects, and allowed an examination of the intrinsic H–mode confinement. Therefore, the DIII–D data was analyzed after the H–mode transition but before the the onset of the first ELM which results in transient confinement analysis. The results presented in this paper are for the ELM-free phase of the JET and DIII–D H–mode and presumably represent optimum H–mode energy confinement.

This paper is organized into four sections. After the introduction in Section 1, the experimental conditions and analysis methods are described in Section 2. The single-null experiments on both tokamaks covered a combined parameter range of toroidal magnetic field between 2.1 T and 2.5 T, $0.8 \leq I_p$ (MA) ≤ 4.5, $1.8 \leq P_b$ (MW) ≤ 13.0, and $2.0 \leq \bar{n}_e(10^{19}\ m^{-3}) \leq 10.0$. The results of an empirical fit and a dimensionally constrained analysis of H–mode confinement are presented in Section 3. Here we find that a power law representation of the H–mode thermal energy confinement implies that $\tau_{th} = C\, I_p^{1.03\pm0.07} P_L^{-0.46\pm0.06} L^{1.48\pm0.09}$ with units of seconds, MA, MW, and meters. The constant of proportionality C is equal to 0.106 ± 0.011 when L is the plasma major radius and is equal to 0.441 ± 0.044 when L is the plasma minor radius. The uncertainty in C and the uncertainties in the I_p,

P_L and R exponents imply an uncertainty in τ_{th} of $\sim$ 18 % for a 2.5 MA, 6 MW, and 2.25 m plasma. The dimensionally constrained analysis assumes that the plasma anomalous transport is determined by a collisional high β model and results in an expression for confinement that is similar to the empirical fit previously stated. Finally, section 4 discusses the implications of our results on L–mode and H–mode scaling relations.

2. EXPERIMENTAL CONDITIONS AND ANALYSIS

The experiments run on both JET and DIII–D were operated in the single-null configuration with an expanded boundary divertor that had the ion ∇B drift towards the X–point. Both plasmas had the same shape as defined by the plasma elongation (1.8), null (0.35) and non–null (0.25) triangularity, X–point distance to the wall (6 cm), and distance between the low field side of the plasma and the wall or limiter (7 cm). The null triangularity is defined for the X–point half of the plasma and the non–null triangularity is defined for the half of the plasma opposite the X–point. Figure 2 shows a poloidal cross–section of both JET and DIII–D, each with a magnetic flux plot of a typical expanded boundary divertor plasma that was operated for this experiment. Both machines were run with 75–80 keV (E_{beam}) deuterium neutral beam injection into a deuterium target plasma. Experiments on DIII–D were run at 2.1 T with a major radius of 1.67 m, a minor radius of 0.62 m, a plasma current range from 0.75 to 2.0 MA, neutral beam power from 1.8 to 10 MW, and a density range from 2.5 to 10.0 $\times$ 10^{19} m^{-3}. There was no ELM free H–mode data obtained at different toroidal fields on DIII–D so that the dependence of H–mode confinement on magnetic field could not be addressed. The JET experiments were carried out between 2.2 and 2.5 T with a major radius of 2.85 m, a minor radius of 1.09 m, a plasma current range from 2.0 to 4.5 MA and neutral beam power between 5 and 10 MW, and a density range from 2.0 to 5.0 $\times$ 10^{19} m^{-3}. In both machines, the global behavior of the H–mode is the same with the L–H transition marked by a rapid decrease in the divertor D_α signal, a rapid increase in the electron density resulting in a flat density profile, and an increase in the energy confinement time. For the majority of the H–mode discharges, the large value of electron density allowed for strong electron–ion

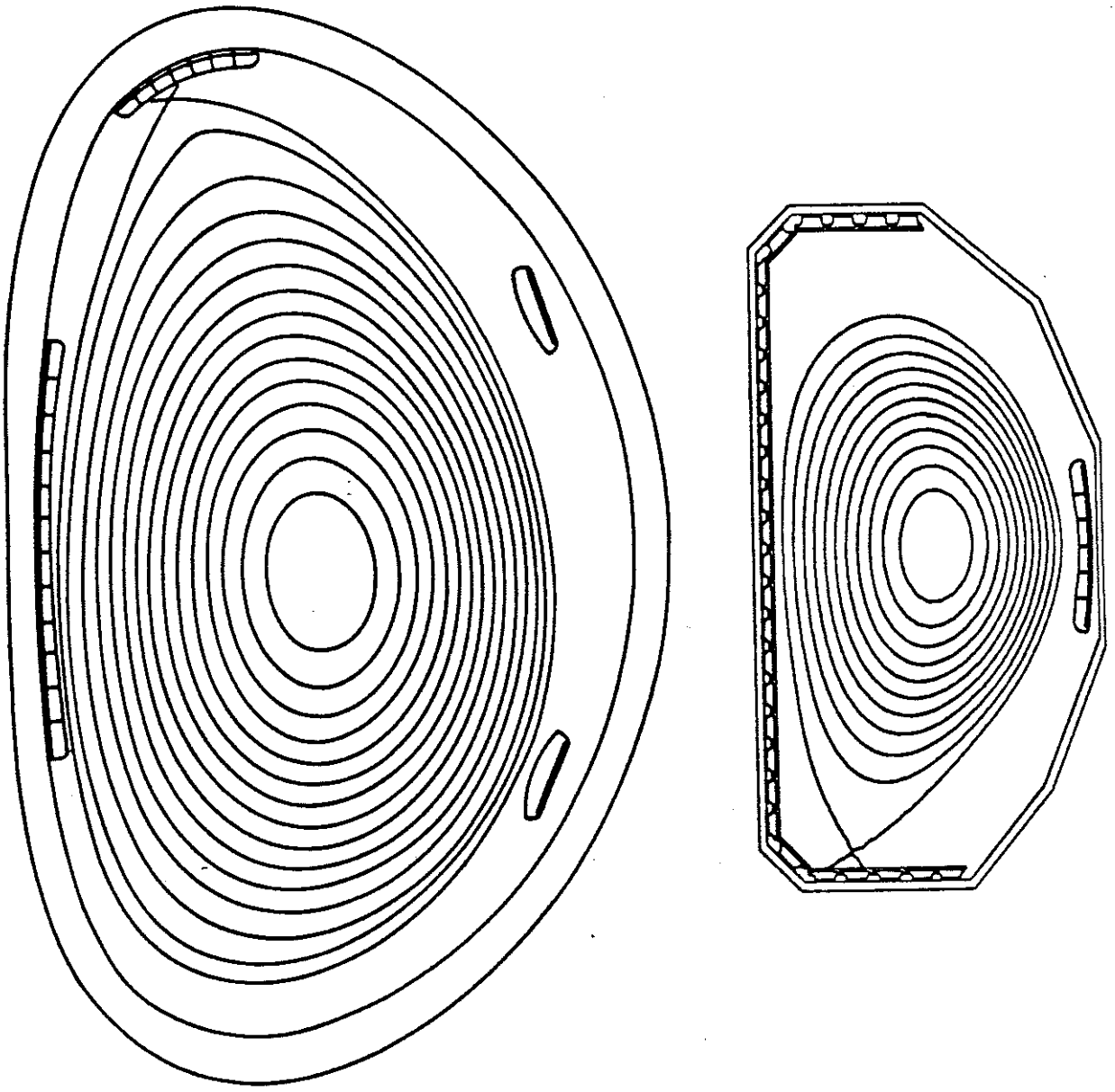

Fig. 2. Poloidal cross–section of the JET and DIII–D tokamaks for an expanded boundary divertor discharge with both machine centers to the left. The figure is drawn to 1/30 scale with $R = 2.85$ m and $a = 1.09$ m for the JET plasma, and $R = 1.67$ m and $a = 0.62$ m for the DIII–D plasma. For JET the two belt limiters are shown on the low field side, the inner wall tiles on the high field side, and the carbon X–point target tiles at the top of the vessel. The DIII–D poloidal cross–section shows the carbon blade limiter on the low field side along with the inner ring of carbon tiles whose function is to protect the inner wall and divertor region.

coupling resulting in similar electron (T_e) and ion (T_i) temperatures. JET data was obtained in the 1986 (2 MA) and 1988 ($\geq$ 3 MA) experimental campaigns, both of which occurred before the introduction of beryllium evaporation. The interior of the JET vessel was carbonized during the 1988 campaign. For the data used in this study, both machines utilized carbon tiles for divertor target area and first wall protection. A comparison of typical JET and DIII–D plasma parameters is shown in Table I.

The previously mentioned parameter ranges for the two tokamaks have a substantial variation in the plasma current, neutral beam power, plasma size, and plasma electron density. Within one machine at fixed plasma current, the accessible range of plasma density in the H–mode was quite limited. In the DIII–D H–mode the electron density and plasma current have been very closely coupled [16]. Attempts to break this coupling have not been successful. It has therefore not been possible on DIII–D to obtain information on how H–mode τ_E varied with both electron density and plasma current. However, results from JET indicated that H–mode τ_E depended only weakly on density [14]. Therefore, in this paper, the dependence of H–mode confinement on n_e has been assumed to be small and was not considered.

In order to insure consistency between the two datasets, it was decided to calculate τ_{th} for both machines at that time in the discharge evolution where $\dot{W}_T/P_T$ had the same value. Using this condition to choose an analysis time guaranteed the calculation of H–mode τ_{th} at the same phase of its temporal evolution regardless of what the evolution path might have been. Furthermore, it was observed for both datasets that the radiated power (P_{rad}) is negatively correlated with $\dot{W}_T$. Therefore, performing confinement analysis at a constant value of $\dot{W}_T/P_T$ implied the same constant value of radiated power for both machines. Possible values of $\dot{W}_T/P_T$ used for this study were limited on the low end by radiation and the onset of ELMs (Fig. 1), and on the high end by the relatively large fast ion contribution to the stored energy increase which occurred just after the neutral beams were switched on. A value of $\dot{W}_T/P_T \approx 0.3$ was chosen as the best compromise and the corresponding time in an

TABLE I
JET/DIII-D COMPARISON

	JET	JET	DIII-D	DIII-D
I_p (MA)	2.0	4.0	0.8	1.9
B_T (T)	2.0	2.5	2.1	2.1
a (m)	1.09	1.09	0.62	0.61
R (m)	2.85	2.85	1.68	1.67
κ	1.8	1.8	1.8	1.8
$T_e(0)$ (keV)	5.5	4.5	3.5	2.9
$T_i(0)$ (keV)	5.5	4.5	7.9	2.7
$\langle n_e \rangle^*(10^{19}$ m$^{-3})$	2.5	4.5	2.7	9.0
$\langle Z_{eff} \rangle^*$	3.0	2.0	2.9	2.0
β_p	0.6	0.3	2.3	0.6
β_T (%)	1.2	1.3	1.5	2.2
$\beta_N^\dagger$ (% T-m/MA)	1.4	0.8	2.5	1.5
W_{fast} (MJ)	0.60	0.30	0.41	0.08
W_{fast}/W_T	0.20	0.05	0.47	0.07
E_{beam}/E_{crit}^{**}	1.2	1.4	1.8	2.2
P_T (MW)	9.0	9.0	7.0	7.7
P_{rad}/P_T	0.3	0.5	0.3	0.4
$\nu_{i*}\|_{\rho=0.9}^\ddagger$ (s^{-1})	0.08	0.16	0.90	1.40
τ_{th} (s)	0.48	1.00	0.09	0.22
τ_{th}/τ_E	0.80	0.95	0.53	0.93

*$\langle\ \rangle$ denotes volume average.

†$\beta_T/(I_p/aB_T)$

**Critical beam slowing down energy

‡Effective ion collision frequency at normalized ρ of 0.9.

H–mode evolution is illustrated by the dotted vertical lines in Fig. 1. This value of $\dot{W}_T/P_T$ implied that the fraction of radiated power was approximately 40% and yielded a database that consisted of 75 JET H–modes and 20 DIII–D H–modes.

The ohmic heating power (P_{OH}) was calculated from plasma resistivity ($\int \eta J^2 dV$) thereby avoiding the need for time dependent analysis of the dynamically evolving loop voltage during the ELM free H–mode phase. Performing confinement analysis at a time such that $\dot{W}_T/P_T$ was non–zero required the calculation to be performed before the discharge had reached steady state. Therefore, the energy confinement time calculated for this study included the correction for the time rate of change of the total stored energy $\tau_E = W_T/\left(P_T - \dot{W}_T\right)$.

The total plasma stored energy was determined from magnetic measurements for JET and DIII–D so that both the beam and thermal energy was included. By measuring the profiles of electron temperature, electron density, ion temperature and Z_{eff}, the DIII–D thermal stored energy (W_{th}) could be separated from the fast ion stored energy (W_{fast}). During the ELM-free phase of the DIII–D H–mode, the low current (low density) discharges had $W_{fast}/W_T \sim 0.45$ and the high current (2 MA) discharges had $W_{fast}/W_T \sim 0.10$. Those 2 MA discharges with insufficient profile information were included in the database by using an expression to calculate the fast ion stored energy ($W_{fast} \sim T_e^{3/2} P_b/n_e$). In this representation of W_{fast}, the volume averaged electron temperature was used for T_e and was obtained from W_T assuming a deuterium dilution factor of unity ($n_d/n_e \sim 1$), and the constant of proportionality was determined from the 2 MA discharges with profile data. Since the percentage of fast ion energy at these currents was small this correction to W_T was also small. The percentage of fast ion energy in the JET H–mode discharges was considerably less and was determined by computer modeling. A full set of kinetic profiles existed for the majority of JET discharges with $I_p \geq 3$ MA. For these plasmas, W_{th} determined by profile integration agreed well with $W_T - W_{fast}$. In the JET computer simulation the fast ion birth profile was determined by using measured plasma profiles and the fast

ion dynamics was modeled by the bounce averaged Fokker–Planck equation. With the calculated thermal stored energy, it was then straightforward to determine a thermal energy confinement time from $\tau_{\rm th} = (W_{\rm th}/W_{\rm T})\,\tau_{\rm E}$. The remainder of this paper will discuss the behavior of the thermal H–mode energy confinement time $\tau_{\rm th}$.

3. H–MODE SCALING RELATIONSHIPS

3.1 Empirical Scaling

Before attempting to establish the dependence of τ_{th} on size for the complete JET/DIII–D dataset, it was essential to assess the dependencies on I_p and P_L for the individual machines. Only if the I_p and P_L dependencies for both machines were the same did it make sense to combine the data to determine a size scaling. Our results indicated that the thermal confinement dependence on I_p and P_L in both machines could be represented by a power law having, within error bars, the same functional form. Therefore, the scaling expressions that follow were performed with an assumed power law dependence of τ_{th} on I_p, P_L, and L. These scalings were obtained using least squares minimization techniques. The error in the exponents were determined by propagating the errors in τ_{th}, estimated to be 15% for both datasets.

The results indicate that when both datasets were examined independently, the thermal energy confinement time was proportional to $I_p^{1.04\pm0.08} P_L^{-0.44\pm0.10}$ for JET and proportional to $I_p^{0.93\pm0.16} P_L^{-0.49\pm0.09}$ for DIII–D. Restricting both datasets to a limited power range ($P_L = 6$ MW) and then examining the current dependence found that τ_{th} was proportional to $I_p^{1.02\pm0.10}$ for JET and $I_p^{0.97\pm0.18}$ for DIII–D (Fig. 3). Fixing the current exponent to unity at the same loss power resulted in a thermal energy confinement quality of 0.227 ± 0.01 s/MA for the JET H–mode and 0.110 ± 0.01 s/MA for DIII–D. The dependence of τ_{th} on the loss power was equally well described either by an offset linear or a power law expression. The power law representation of τ_{th} for the 2.0 MA H–mode discharges is shown for both datasets

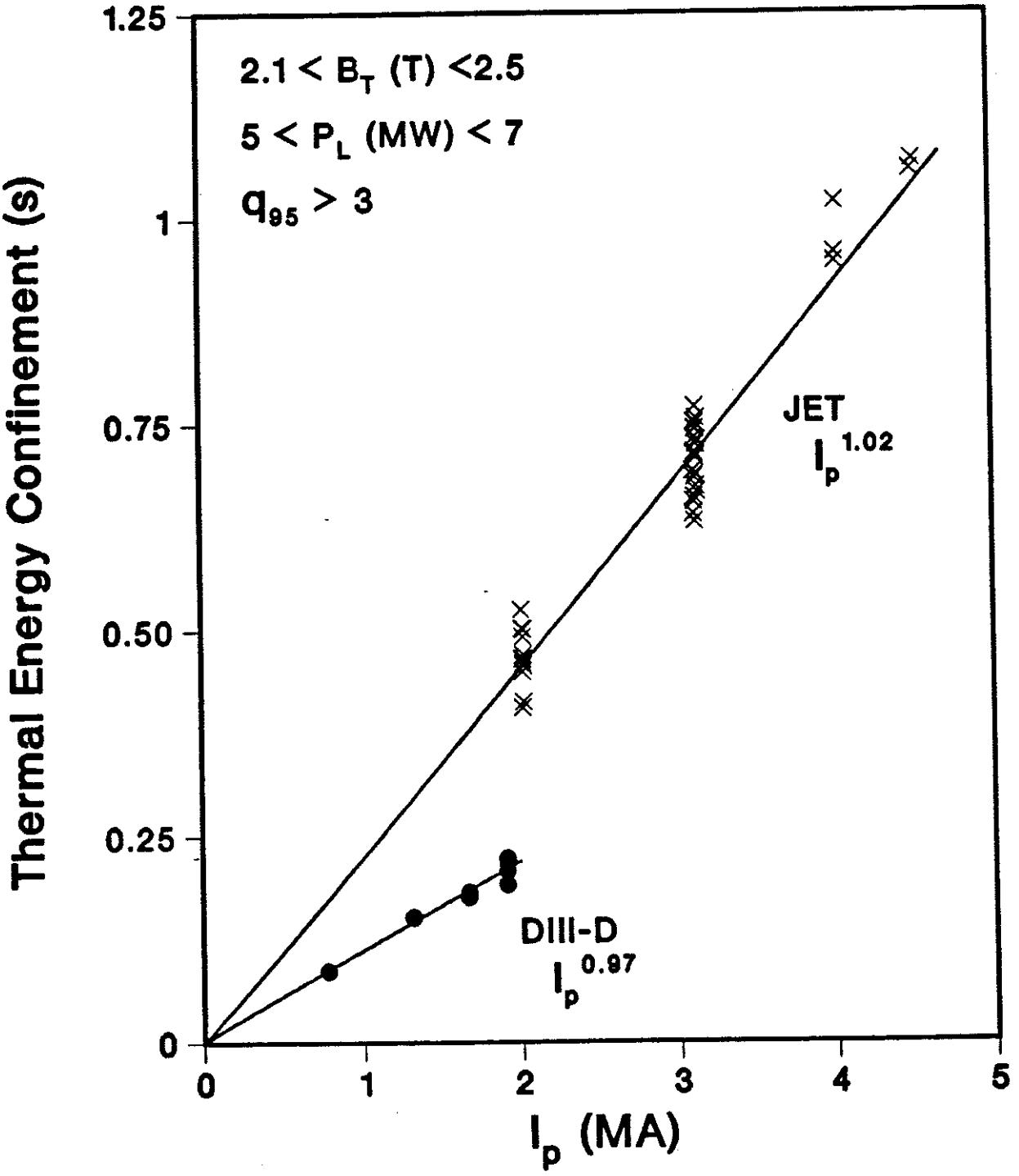

Fig. 3. ELM-free H–mode thermal energy confinement versus plasma current for DIII–D and JET for data in a narrow range of power. The two solid lines represent a least squares fit to the restricted data set for each tokamak assuming a power law functional form.

in Fig. 4. Here it was found that τ_{th} was proportional to $P_L^{-0.50\pm0.10}$ for DIII–D and $P_L^{-0.49\pm0.17}$ for JET.

Fitting the entire database of JET and DIII–D H–mode discharges and assuming that τ_{th} depended only on I_p, P_L, and L (recall B_T, κ, R/a , and m_i were held constant) resulted in the following expression for the thermal energy confinement of an ELM-free H–mode

$$\tau_{th}\ (\mathrm{sec}) = C\, I_p^{\,1.03\pm0.07}\, P_L^{-0.46\pm0.06}\, L^{1.48\pm0.09} \quad . \tag{1}$$

The coefficient $C = 0.106 \pm 0.011$ for $L = R$ and $C = 0.441 \pm 0.044$ when $L = a$ where I_p is in MA, P_L is in MW and L is in meters. This H–mode scaling relationship describes thermal energy confinement in an ELM-free divertor deuterium H–mode with $B_T \approx 2.2$ T, $\kappa = 1.8$ and $R/a \approx 2.65$. Figure 5 shows both DIII–D and JET τ_{th}, normalized by the I_p and P_L dependence ($\tau_{th} P_L^{\,0.46} / I_p^{\,1.03}$), plotted versus plasma major radius. The solid line in the figure represents the inferred size dependence of τ_{th}. Figure 6 shows the experimentally measured τ_{th} versus that predicted by Eq. (1). The correlation coefficients for the data used to derive Eq. (1) are 0.30 for R–P_L, 0.44 for I_p–P_L, and 0.57 for I_p–R. These results indicate that to within a 1% level of significance no correlation existed between R and P_L but there was some correlation between the other two pairs. The experimental correlation coefficients of I_p–P_L, and I_p–R are sufficiently small that it is justifiable to assume that they are independent variables in this model. The uncertainty in τ_{th} can be estimated by using only the four diagonal elements of the covariance matrix. This technique yields an uncertainty in τ_{th} of $\sim$ 18 % for a plasma residing in the middle of the I_p, P_L and R ranges (2.5 MA, 6 MW, 2.25 m) used in this study.

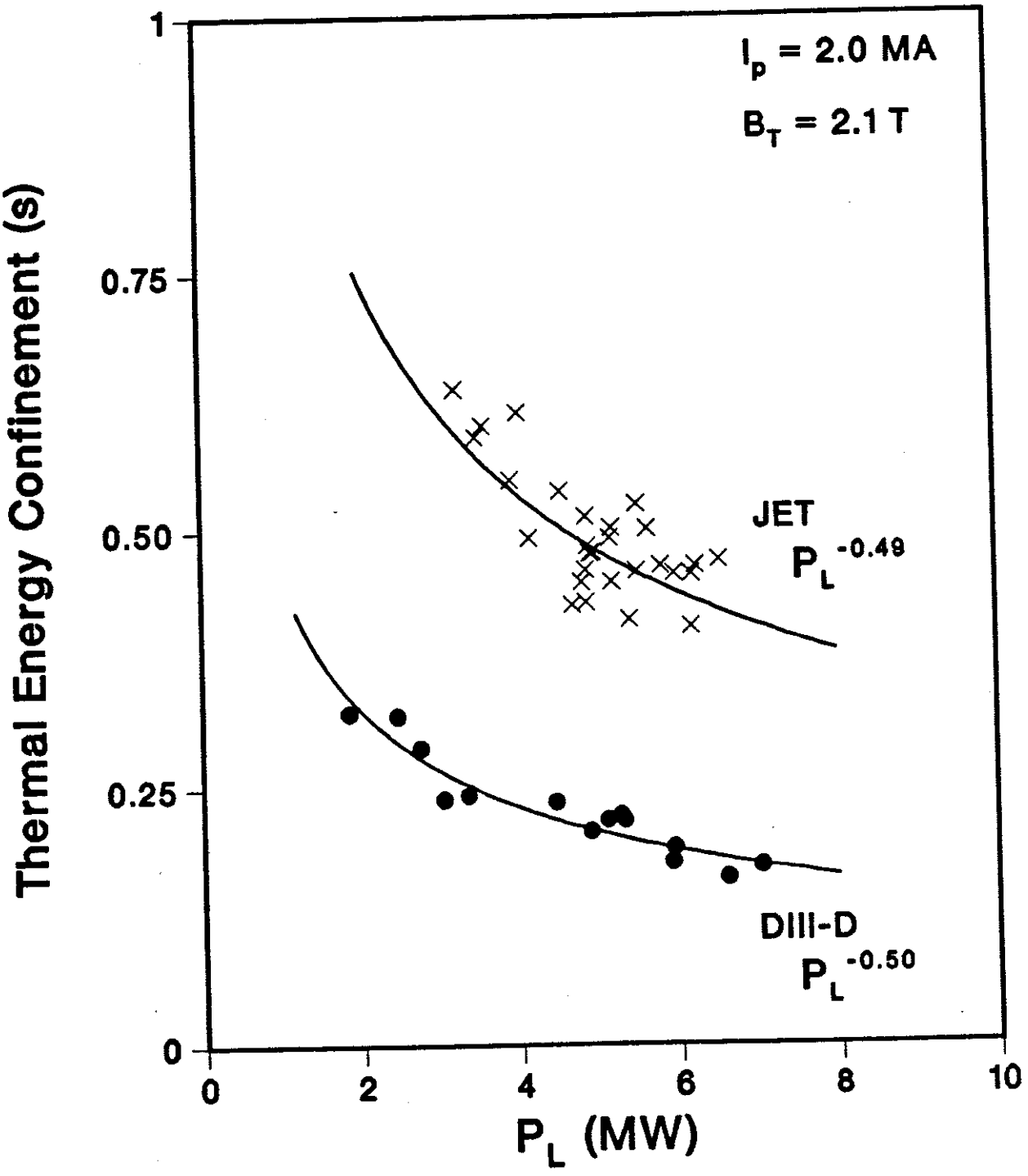

Fig. 4. ELM-free 2 MA H–mode thermal energy confinement versus loss power for JET and DIII–D. The two solid lines represent a least squares fit to the restricted data set for each tokamak assuming a power law functional form.

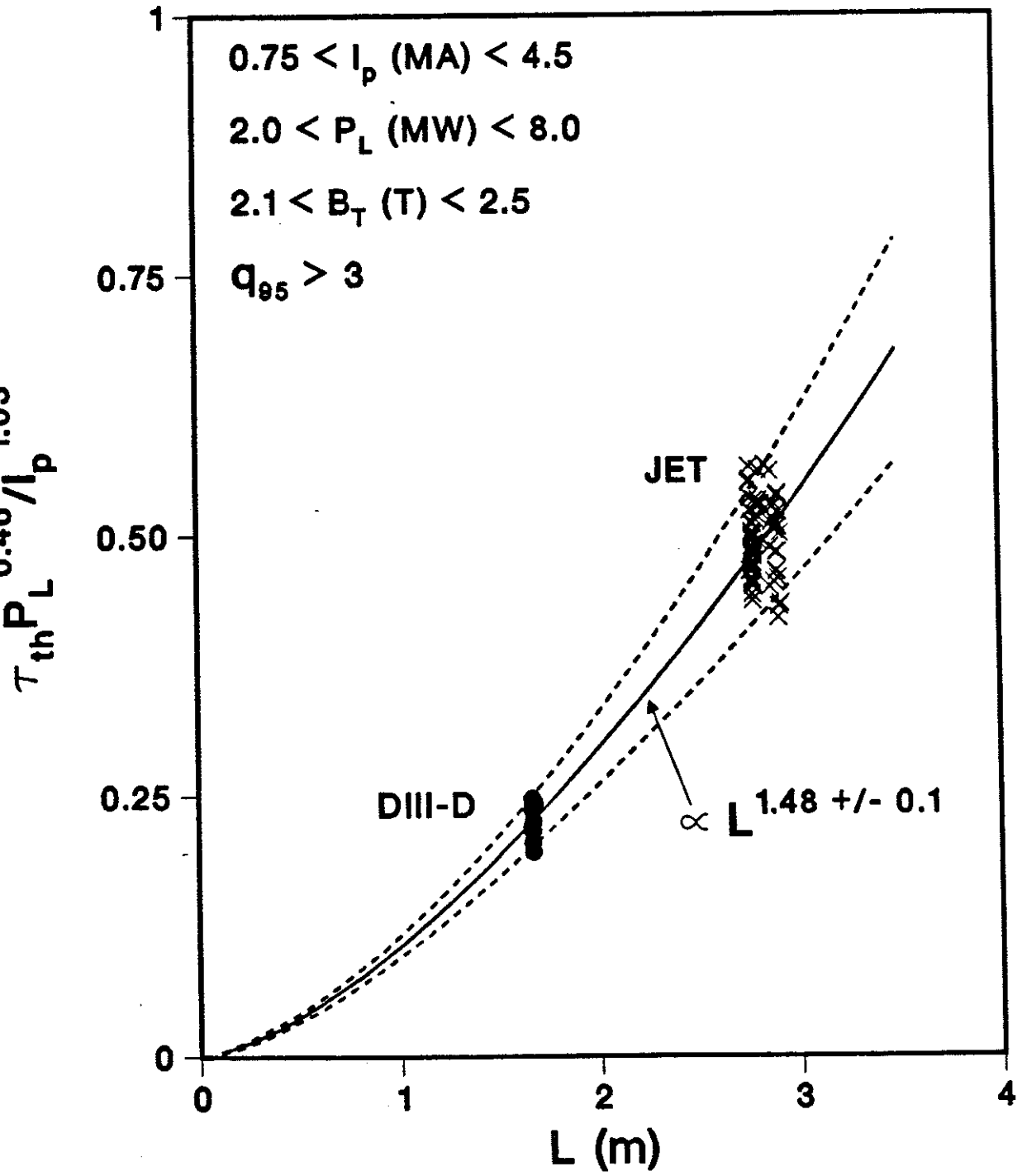

Fig. 5. Normalized ELM-free H–mode thermal energy confinement versus plasma size for the entire database. The solid line represents a least squares fit to the data. The dashed lines represent the one standard deviation error associated with the fit.

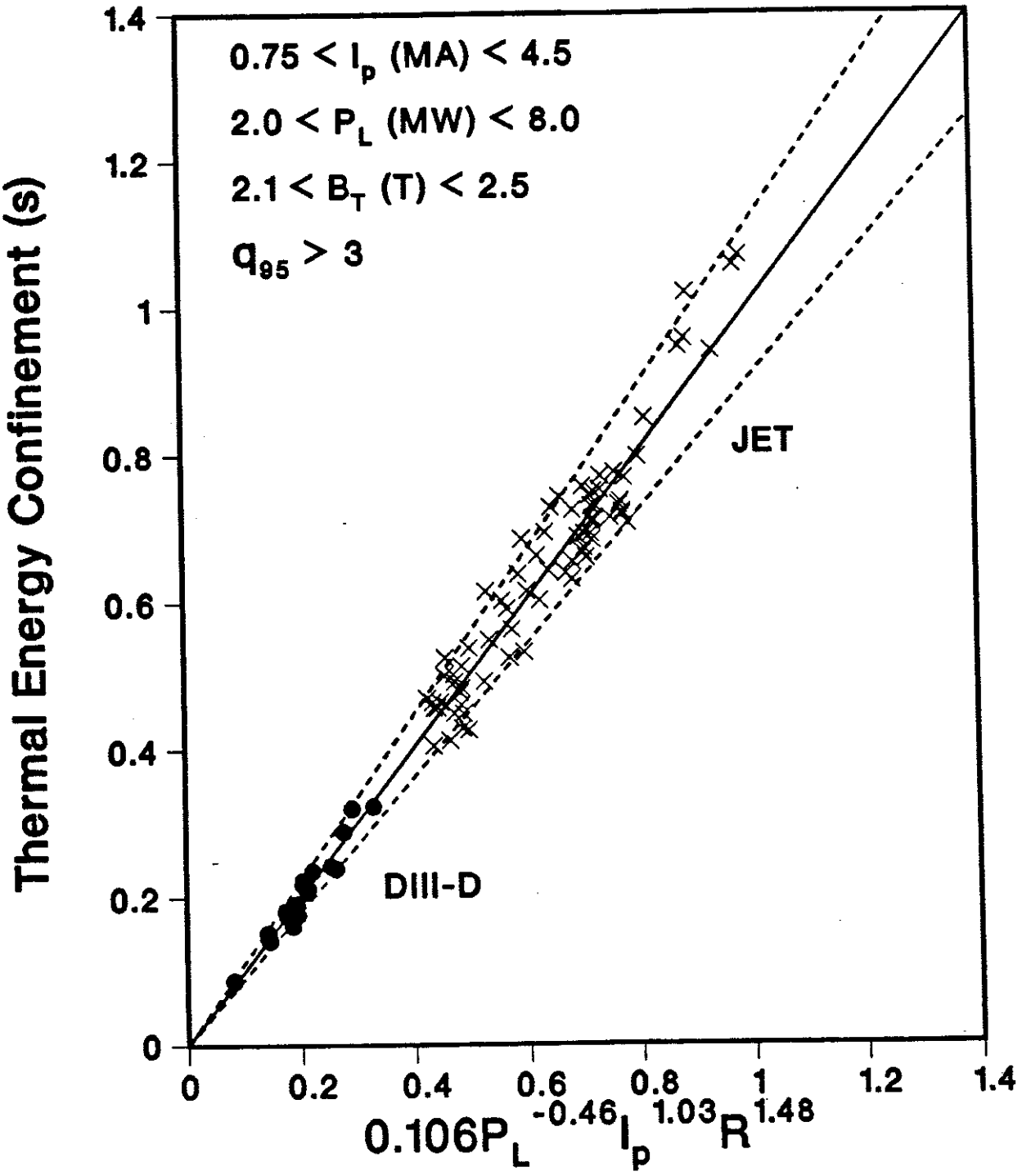

Fig. 6. Experimentally determined ELM-free H–mode thermal energy confinement versus the values derived from Eq. (1). The solid line has a slope of unity and is plotted for comparison only. The dashed lines represent a 10% deviation from the solid line. Equation 1 was obtained from DIII–D and JET deuterium H–mode data with $B_T \approx 2.2$ T, $\kappa = 1.8$ and $R/a \approx 2.65$.

3.2 Dimensionless Scaling

It is well known that for any particular model of anomalous transport the Invariance Principle constrains the form of confinement scaling in a manner that is characteristic of that model. This approach, recently reviewed by Connor [17], leads to the formulation of a set of dimensionless parameters, which are characteristic of the selected set of basic equations. If it is assumed that the anomalous transport is governed by the equations of a collisional high β model such as the quasi–neutral high β Fokker–Planck equation, it follows that the energy confinement should be described by the dimensionless parameters $\tau_{\rm th}/\tau_{\rm N}$, β_p, $\hat{\nu}$, and ρ_p/L. Here $\tau_{\rm N}$ is the normalization time defined by $L/v_{\rm th}$, $v_{\rm th}$ is the electron thermal velocity, β_p is the poloidal beta, $\hat{\nu}$ is the normalized collision frequency defined by $\nu_{ei}/\left(c_s/L\right)$, and ρ_p is the poloidal Larmor radius. In an alternative formulation, due to Rebut and Brusati [4,18], the dimensionless parameters are $\tau_{\rm th}/\tau_{\rm N}$, β_p, $\Omega \propto \left(\rho_p/L\right)^2$, and $\Delta \propto \eta J/\left(B_p v_{\rm th}\right)$. In each representation these dimensionless parameters are supplemented by a set of shape parameters such as q, R/a, m_i/m_e, κ, and $\mathrm{Z_{eff}}$. For the present analysis the q dependence has been added to the description of energy confinement. Recall that R/a, m_i/m_e, and κ were constant for the JET/DIII–D data used to derive Eq. (1). The dimensionless expressions have been written in a power law form since this representation accurately described the data in the empirical fit. Therefore, with the preceding assumptions, the energy confinement can be written as

$$\tau_{\rm th}/\tau_{\rm N} \propto \beta_p^{\gamma_\beta}\ \hat{\nu}^{\gamma_\nu}\ \left(\rho_p/L\right)^{\gamma_\rho}\ q^{\gamma_q} \quad . \tag{2}$$

or

$$\tau_{\rm th}/\tau_{\rm N} \propto \beta_p^{\gamma'_\beta}\ \Omega^{\gamma_\Omega}\ \Delta^{\gamma_\Delta}\ q^{\gamma_q} \quad . \tag{3}$$

The exponents of Eqs (2) and (3) are related by $\gamma'_\beta = \gamma_\beta + \gamma_\nu$, $\gamma_\Omega = \gamma_\rho/2 - \gamma_\nu$, and $\gamma_\Delta = \gamma_\nu$.

Dimensionally correct scalings can be constructed from empirical scalings following a procedure outlined by Christiansen [19]. The empirical scaling for confinement can be written as

$$\tau_{\rm th} \propto {\rm I_p^{\alpha_I}}\ P_L^{\alpha_P}\ L^{\alpha_L}\ {\rm B_T^{\alpha_B}}\ n_e^{\alpha_n} \tag{4}$$

where for the JET/DIII–D dataset the density dependence has been assumed negligible ($\alpha_n = 0$). Equation (2) or (3) can be rewritten in terms of characteristic plasma parameters as

$$\tau_{\rm th} \propto {\rm I_p^{\delta_I}}\ P_L^{\delta_P}\ L^{\delta_L}\ {\rm B_T^{\delta_B}}\ n_e^{\delta_n} \quad . \tag{5}$$

It is then a simple matter to solve for the δ's of Eq. (5) given the α's in Eq. (4). This solution is obtained by minimizing the sum of the squares of the residuals between the values of α in Eq. (4) and the corresponding δ in Eq. (5) which are functions of the γ's in Eqs. (2) or (3). Equation (1) provides the values of α except for α_B which was not determined in the empirical scaling. Separately determining the γ's of Eqs. (2) and (3) and carrying the α_B dependence along results in a dimensionless scaling of

$$\tau_{\rm th}/\tau_{\rm N} \propto \beta_p^{-0.33-0.42\alpha_B}\ \hat{\nu}^{-0.35-0.25\alpha_B}\ (\rho_p/L)^{-1.38-0.50\alpha_B}\ q^{0.107+1.43\alpha_B} \tag{6}$$

and

$$\tau_{\rm th}/\tau_{\rm N} \propto \beta_p^{-0.68-0.67\alpha_B}\, \Omega^{-0.34}\, \Delta^{-0.35-0.25\alpha_B}\, q^{0.107+1.43\alpha_B} \quad . \tag{7}$$

As has been stated earlier, the database used to derive Eq. (1) had a very limited range in B_T and therefore the value of α_B was not determined. Limiting values for α_B of 0 and 0.5 can be inferred from existing data. DIII–D confinement data [16] taken in the presence of ELMs indicated that τ_E did not depend on B_T. JET results [14] reported that ELM free τ_E depended on toroidal field as $B_T^{0.48}$, although a smaller B_T dependence is supported by more recent data. Therefore, Eqs. (6) and (7) with $\alpha_B = 0$ become

$$\tau_{\rm th} \propto I_p^{1.06}\, P_L^{-0.45}\, L^{1.40}\, n_e^{0.07}\, B_T^{0.06} \tag{8}$$

and with $\alpha_B = 0.5$ become

$$\tau_{\rm th} \propto I_p^{1.00}\, P_L^{-0.47}\, L^{1.55}\, n_e^{-0.07}\, B_T^{0.43} \quad . \tag{9}$$

Both results indicate that having a small dependence of $\tau_{\rm th}$ on n_e and a B_T dependence between 0 and 0.5 is consistent with the dimensionless analysis. Furthermore, Eqs. (8) and (9), within the indicated experimental error, are identical to the empirical fit of Eq. (1).

4. DISCUSSION

As was stated in the introduction, predictions for H–mode confinement have been based on L–mode scaling expressions times an H–mode improvement factor of order two. One such L–mode scaling, based on a power law representation, was developed by Goldston [3]. It is interesting to note the similar functional dependencies of τ_E on I_p, P_T, and L in the Goldston expression ($I_p^{1.0} P_T^{-0.5} L^{1.38}$) to that in Eq. (1). The H–mode scaling of Eq. (1) represents, on average for our database, a factor of 1.8 improvement over the τ_E predicted by Goldston scaling. A recent addition to Goldston scaling has been to add a mass dependence in terms of $M_{eff}^{1/2}$, where M_{eff} is taken to be the average of the plasma and beam species. With this additional mass factor the H–mode multiplier drops to 1.6. However, since L–mode τ_E has been shown to be independent of ion mass for both JET [20] and DIII–D [16] , this addition to Goldston scaling is questionable.

An example of a global scaling expression based on an offset linear representation, where the numerical coefficients have been optimized for JET ohmic and L-mode data, has been developed by Rebut and Lallia [4]. This scaling for electron confinement is $\tau_{E,e} = 0.012\, I_p\, L^{1.5}\, Z_{eff}^{-0.5} + 0.026\, n_e^{0.75}\, I_p^{0.5}\, B_T^{0.5}\, L^{2.75}\, Z_{eff}^{0.25}\, P_L^{-1.0}$. Application to our database indicates an overall H–mode multiplier of about 1.6, where the electron confinement time is taken as $\tau_E/2$. The plasma size effect in the Rebut–Lallia scaling is well represented at higher power levels ($P_L \geq 4$ MW). There is a systematic effect with plasma current in particular for JET; the scaling underestimates the confinement of the 3 MA H–modes relative to those at 2 MA and 4 MA, by about 25%. The scaling overestimates the confinement of the lower power DIII–D data ($P_L \leq 4$ MW) by up to a factor of 2. The deviations are perhaps not so surprising

since the global Rebut–Lallia scaling, as an approximation to a local transport model, does not take into account differences between T_e and T_i, the dilution, the profiles and the edge related H–mode enhancement.

Recently the ITER team [21] has attempted to unify the large number of L–mode scaling expressions by enhancing the existing L–mode database and creating the ITER–89 L–mode power law fit ($\tau_E^{IP} \sim I_p^{0.85} P_T^{-0.5} L^{1.5} M_{eff}^{0.5}$). This expression has then been used to estimate ITER H–mode confinement by using ~ 2 for the H–mode enhancement. This factor compares favorably to the average of 1.8 improvement for our database that Eq. (1) predicts over τ_E^{IP}. The auxiliary power and size dependencies of the ITER–89 fit are similar to the H–mode expression developed in this paper but the current dependence is somewhat weaker. Early DIII–D [16] H–mode results with ELMs indicated that deuterium confinement was twice hydrogen confinement. This result combined with the H–mode confinement similarity of hydrogen and helium indicated that the scaling of H–mode τ_E with ion species was not described by the ion mass (m_i) alone. The similar hydrogen and helium H–mode confinement suggested that the proper scaling may be a function of m_i/Z_i^2. More recently, the hydrogen H–mode was obtained on DIII–D [22] with a smaller ELM frequency and a larger τ_E than was previously achieved which indicated that deuterium τ_E was only $\sim \sqrt{2}$ larger than the τ_E in hydrogen. Therefore, for scaling expressions like Goldston or ITER–89 that are used to predict hydrogen and deuterium H–mode confinement, $\tau_E \sim \sqrt{m_i}$ would properly represent DIII–D data. Since no recent helium H–modes have been attempted it is not possible to comment on whether $\sqrt{m_i}/Z_i$ might better describe the scaling of τ_E with ion species.

In conclusion, an empirical H–mode τ_{th} scaling study based on JET and DIII–D H–mode data has found that $\tau_{th} \sim I_p^{1.03\pm0.07} P_L^{-0.46\pm0.06} L^{1.48\pm0.09}$. The dependence of τ_{th} on B_T, κ, R/a, and m_i was not investigated since these parameters were not varied in this study. A dimensionally correct version of this scaling, consistent with a collisional high β model, is $\tau_{th} \sim I_p^{1.06} P_L^{-0.45} L^{1.40} n_e^{0.07} B_T^{0.06}$ assuming $\tau_{th} \sim B_T^0$

and is $\tau_{th} \sim I_p^{1.00} P_L^{-0.47} L^{1.55} n_e^{-0.07} B_T^{0.43}$ assuming $\tau_{th} \sim B_T^{0.5}$. The differences in these dimensionally constrained scalings represent the uncertainty in the dependence of τ_{th} on toroidal field since a B_T scan was not performed. These results presumably represent the optimum H–mode confinement since only the ELM free phase of the H–mode has been examined. These H–mode scaling expressions were obtained at constant elongation (1.8), toroidal field ($\approx$ 2.2 T), aspect ratio ($\approx$ 2.65), and ion species (deuterium), with the consequence that the effect of these parameters on τ_{th} was not determined. The resulting scaling is remarkably close in the functional dependencies on the independent variables to the Goldston and ITER–89 scalings. Thus, although the application of L–mode scaling for H–mode predictions is not necessarily logically consistent, this justifies to a large extent the predictions that have been made.

REFERENCES

[1] POST, D., in Plasma Physics and Controlled Nuclear Fusion Research 1988 (Proc. 12th Int. Conf. Nice, 1988), Vol. 3, IAEA, Vienna (1989) 233.

[2] KAYE, S.M., GOLDSTON, R.J., Nucl. Fusion **25** (1985) 65.

[3] GOLDSTON, R.J., Plasma Physics and Controlled Fusion **26** (1984) 87.

[4] REBUT, P.H., LALLIA, P.P., WATKINS, M.L., in Plasma Physics and Controlled Nuclear Fusion Research 1988 (Proc. 12th Int. Conf. Nice, 1988), Vol. 2, IAEA, Vienna (1989) 191.

[5] ODAJIMA, K., SHIMOMURA, Y., Energy Confinement Scaling based on Offset Linear Characteristic, Japan Atomic Energy Research Institute Report JAERI–M 88–068 (1988).

[6] WAGNER, F., BECKER, G., BEHRINGER, K., CAMPBELL, D., EBERHAGEN, A., *et al.*, Phys. Rev. Lett. **49** (1982) 1408.

[7] TANGA, A., BARTLETT, D.V., BEHRINGER, K., BICKERTON, R.J., CHEETHAM, A., *et al.*, in Plasma Physics and Controlled Nuclear Fusion Research 1986 (Proc. 11th Int. Conf. Kyoto, 1986), Vol. 1, IAEA, Vienna (1987) 65.

[8] SUZUKI, N., MIURA, Y., HASEGAWA, M., HOSHINO, K., KASAI, S., *et al.*, *in Proceedings of the Fourteenth European Conference on Controlled Fusion and Plasma Physics, Madrid, Spain,* 1987 (European Physical Society, Petit-Lancy, Switzerland, 1987), Vol. 11D, part II, p. 217.

[9] KAYE, S.M., BELL, M.G., BOL, K., BOYD, D., BRAU, D., *et al.*, J. Nucl. Mater. **121** (1984) 115.

[10] BURRELL, K.H., EJIMA, S., SCHISSEL, D.P., BROOKS, N.H., CALLIS, R.W., *et al.*, Phys. Rev. Lett. **59** (1987) 1432.

[11] WATKINS, M., BALET, B., BHATNAGAR, V.P., *et al.*, Plasma Physics and Controlled Fusion **31** (1989) 1713.

[12] BURRELL, K.H., GROEBNER, R.J., CARLSTROM, T.N., *et al.*, Comparison of Thermal and Angular Momentum Transport in Neutral Beam–Heated Hot–Ion H– and L–mode Discharges in DIII–D, Rep. GA–A20058, General Atomics, San Diego, CA (1990), to be published *in Proceedings of the Seventeenth European Conference on Controlled Fusion and Plasma Physics, Amsterdam, The Netherlands.*

[13] BURRELL, K.H, ALLEN, S.L., BRAMSON, G., *et al.*, Plasma Physics and Controlled Fusion **31** (1989) 1649.

[14] JET TEAM, in Plasma Physics and Controlled Nuclear Fusion Research 1988 (Proc. 12th Int. Conf. Nice, 1988), Vol. 1, IAEA, Vienna (1989) 159.

[15] MAHDAVI, M.A., KELLMAN, A., GOHIL, P., BROOKS, N., BURRELL, K.H., *et al., in Proceedings of the Sixteenth European Conference on Controlled Fusion and Plasma Physics, Venice, Italy,* 1989 (European Physical Society, Petit-Lancy, Switzerland, 1989), Vol. 13B, part I, p. 249.

[16] SCHISSEL, D.P., BURRELL, K.H., DEBOO, J.C, *et al.*, Nucl. Fusion **29** (1989) 185.

[17] CONNOR, J.W., Plasma Physics and Controlled Fusion **30** (1988) 619.

[18] REBUT, P.H., BRUSATI, M., Plasma Physics and Controlled Fusion **28** (1986) 113.

[19] CHRISTIANSEN, J.P., CORDEY, J.G., THOMSEN, K., A Unified Physical Scaling Law for Tokamak Energy Confinement, JET-P(90)05 (1989), Jet Joint Undertaking, accepted for publication in Nucl. Fusion.

[20] CORDEY, J.G., BARTLETT, D.V., BHATNAGAR, V., BICKERTON, R.J., BURES, M., *et al.*, in Plasma Physics and Controlled Nuclear Fusion Research 1986 (Proc. 11th Int. Conf. Kyoto, 1986), Vol. 1, IAEA, Vienna (1987) 99.

[21] ITER TEAM, "ITER Conceptual Design – Interim Report," IAEA, Vienna (1989).

[22] DEBOO, J.C., SCHISSEL, D.P., BURRELL, K.H., ST JOHN, H., Initial Deuterium Confinement Studies in DIII–D Tokamak: DIII–D Milestone Report # 58, Rep. GA–A19803, General Atomics, San Diego, CA (1989).

ACKNOWLEDGMENTS

The authors are greatly indebted to members of the JET Team and the DIII–D Research Team and, in particular, to the diagnosticians who have made their data available to them. The comments of Drs. Rebut and Watkins from JET are greatly appreciated. Also appreciated are the numerous valuable discussions held with Dr. Taylor from DIII–D while he was on assignment at JET. Two of the authors (D.P.S. and J.C.D.) would like to acknowledge the generous hospitality of the JET Team during their stay at the JET Joint Undertaking. This joint effort was carried out under an "Agreement for Cooperation between the European Atomic Energy Community and the United States Department of Energy in the Field of Controlled Thermonuclear Fusion." The work of the DIII–D Research Team was supported by the U.S. Department of Energy under Contract No. DE-AC03-89ER51114.

APPENDIX 1.

THE JET TEAM

JET Joint Undertaking, Abingdon, Oxon, OX14 3EA, U.K.

J.M.Adams[1], F.Alladio[4], H.Altmann, R.J.Anderson, G.Appruzzese, W.Bailey, B.Balet, D.V.Bartlett, L.R.Baylor[24], K.Behringer, A.C.Bell, P.Bertoldi, E.Bertolini, V.Bhatnagar, R.J.Bickerton, A.Boileau[3], T.Bonicelli, S.J.Booth, G.Bosia, M.Botman, D.Boyd[31], H.Brelen, H.Brinkschulte, M.Brusati, T.Budd, M.Bures, T.Businaro[4], H.Buttgereit, D.Cacaut, C.Caldwell-Nichols, D.J.Campbell, P.Card, J.Carwardine, G.Celentano, P.Chabert[27], C.D.Challis, A.Cheetham, J.Christiansen, C.Christodoulopoulos, P.Chuilon, R.Claesen, S.Clement[30], J.P.Coad, P.Colestock[6], S.Conroy[13], M.Cooke, S.Cooper, J.G.Cordey, W.Core, S.Corti, A.E.Costley, G.Cottrell, M.Cox[7], P.Cripwell[13], F.Crisanti[4], D.Cross, H.de Blank[16], J.de Haas[16], L.de Kock, E.Deksnis, G.B.Denne, G.Deschamps, G.Devillars, K.J.Dietz, J.Dobbing, S.E.Dorling, P.G.Doyle, D.F.Düchs, H.Duquenoy, A.Edwards, J.Ehrenberg[14], T.Elevant[12], W.Engelhardt, S.K.Erents[7], L.G.Eriksonn[5], M.Evrard[2], H.Falter, D.Flory, M.Forrest[7], C.Froger, K.Fullard, M.Gadeberg[11], A.Galetsas, R.Galvao[8], A.Gibson, R.D.Gill, A.Gondhalekar, C.Gordon, G.Gorini, C.Gormezano, N.A.Gottardi, C.Gowers, B.J.Green, F.S.Griph, M.Gryzinski[26], R.Haange, G.Hammett[6], W.Han[9], C.J.Hancock, P.J.Harbour, N.C.Hawkes[7], P.Haynes[7], T.Hellsten, J.L.Hemmerich, R.Hemsworth, R.F.Herzog, K.Hirsch[14], J.Hoekzema, W.A.Houlberg[24], J.How, M.Huart, A.Hubbard, T.P.Hughes[32], M.Hugon, M.Huguet, J.Jacquinot, O.N.Jarvis, T.C.Jernigan[24], E.Joffrin, E.M.Jones, L.P.D.F.Jones, T.T.C.Jones, J.Källne, A.Kaye, B.E.Keen, M.Keilhacker, G.J.Kelly, A.Khare[15], S.Knowlton, A.Konstantellos, M.Kovanen[21], P.Kupschus, P.Lallia, J.R.Last, L.Lauro-Taroni, M.Laux[33], K.Lawson[7], E.Lazzaro, M.Lennholm, X.Litaudon, P.Lomas, M.Lorentz-Gottardi[2], C.Lowry, G.Magyar, D.Maisonnier, M.Malacarne, V.Marchese, P.Massmann, L.McCarthy[28], G.McCracken[7], P.Mendonca, P.Meriguet, P.Micozzi[4], S.F.Mills, P.Millward, S.L.Milora[24], A.Moissonnier, P.L.Mondino, D.Moreau[17], P.Morgan, H.Morsi[14], G.Murphy, M.F.Nave, M.Newman, L.Nickesson, P.Nielsen, P.Noll, W.Obert, D.O'Brien, J.O'Rourke, M.G.Pacco-Düchs, M.Pain, S.Papastergiou, D.Pasini[20], M.Paume[27], N.Peacock[7], D.Pearson[13], F.Pegoraro, M.Pick, S.Pitcher[7], J.Plancoulaine, J-P.Poffé, F.Porcelli, R.Prentice, T.Raimondi, J.Ramette[17], J.M.Rax[27], C.Raymond, P-H.Rebut, J.Removille, F.Rimini, D.Robinson[7], A.Rolfe, R.T.Ross, L.Rossi, G.Rupprecht[14], R.Rushton, P.Rutter, H.C.Sack, G.Sadler, N.Salmon[13], H.Salzmann[14], A.Santagiustina, D.Schissel[25], P.H.Schild, M.Schmid, G.Schmidt[6], R.L.Shaw, A.Sibley, R.Simonini, J.Sips[16], P.Smeulders, J.Snipes, S.Sommers, L.Sonnerup, K.Sonnenberg, M.Stamp, P.Stangeby[19], D.Start, C.A.Steed, D.Stork, P.E.Stott, T.E.Stringer, D.Stubberfield, T.Sugie[18], D.Summers, H.Summers[20], J.Taboda-Duarte[22], J.Tagle[30], H.Tamnen, A.Tanga, A.Taroni, C.Tebaldi[23], A.Tesini, P.R.Thomas, E.Thompson, K.Thomsen[11], P.Trevalion, M.Tschudin, B.Tubbing, K.Uchino[29], E.Usselmann, H.van der Beken, M.von Hellermann, T.Wade, C.Walker, B.A.Wallander, M.Walravens, K.Walter, D.Ward, M.L.Watkins, J.Wesson, D.H.Wheeler, J.Wilks, U.Willen[12], D.Wilson, T.Winkel, C.Woodward, M.Wykes, I.D.Young, L.Zannelli, M.Zarnstorff[6], D.Zasche[14], J.W.Zwart.

PERMANENT ADDRESS

1. UKAEA, Harwell, Oxon. UK.
2. EUR-EB Association, LPP-ERM/KMS, B-1040 Brussels, Belgium.
3. Institute National des Récherches Scientifique, Quebec, Canada.
4. ENEA-CENTRO Di Frascati, I-00044 Frascati, Roma, Italy.
5. Chalmers University of Technology, Göteborg, Sweden.
6. Princeton Plasma Physics Laboratory, New Jersey, USA.
7. UKAEA Culham Laboratory, Abingdon, Oxon. UK.
8. Plasma Physics Laboratory, Space Research Institute, Sao José dos Campos, Brazil.
9. Institute of Mathematics, University of Oxford, UK.
10. CRPP/EPFL, 21 Avenue des Bains, CH-1007 Lausanne, Switzerland.
11. Risø National Laboratory, DK-4000 Roskilde, Denmark.
12. Swedish Energy Research Commission, S-10072 Stockholm, Sweden.
13. Imperial College of Science and Technology, University of London, UK.
14. Max Planck Institut für Plasmaphysik, D-8046 Garching bei München, FRG.
15. Institute for Plasma Research, Gandhinagar Bhat Gujat, India.
16. FOM Instituut voor Plasmafysica, 3430 Be Nieuwegein, The Netherlands.
17. Commissiariat à L'Energie Atomique, F-92260 Fontenay-aux-Roses, France.
18. JAERI, Tokai Research Establishment, Tokai-Mura, Naka-Gun, Japan.
19. Institute for Aerospace Studies, University of Toronto, Downsview, Ontario, Canada.
20. University of Strathclyde, Glasgow, G4 ONG, U.K.
21. Nuclear Engineering Laboratory, Lapeenranta University, Finland.
22. JNICT, Lisboa, Portugal.
23. Department of Mathematics, Univeristy of Bologna, Italy.
24. Oak Ridge National Laboratory, Oak Ridge, Tenn., USA.
25. G.A. Technologies, San Diego, California, USA.
26. Institute for Nuclear Studies, Swierk, Poland.
27. Commissiariat à l'Energie Atomique, Cadarache, France.
28. School of Physical Sciences, Flinders University of South Australia, South Australia SO42.
29. Kyushi University, Kasagu Fukuoka, Japan.
30. Centro de Investigaciones Energeticas Medioambientales y Techalogicas, Spain.
31. University of Maryland, College Park, Maryland, USA.
32. University of Essex, Colchester, UK.
33. Akademie de Wissenschaften, Berlin, DDR.

CR 88.49.1A